POLITECNICO DI TORINO
Repository ISTITUZIONALE

Non-Invasive Measurements and FEM Analyses for Estimating the Rotor Bar-Lamination Contact
Resistance

(Article begins on next page)

11 April 2024

Non-Invasive Measurements and FEM Analyses for Estimating the Rotor Bar-Lamination Contact Resistance

Zbigniew Gmyrek, Silvio Vaschetto, *Senior Member*, *IEEE*,
Mostafa Ahmadi Darmani, *Student Member, IEEE*, and Andrea Cavagnino, *Fellow IEEE*

Abstract—**This research work investigates the phenomena of inter-bar currents in induction motors equipped with die-cast aluminum cages. Flowing in the lamination and distorting the bar current distributions, the inter-bar currents cause additional stray losses, as well as increase of the Joule loss in the cage bars. The contact resistance between the bars and the rotor laminations is the key modeling element for a correct prediction of the inter-bar currents and the related extra losses.**

The study presents a new non-invasive method to obtain a reliable estimation of the contact resistance. The proposed '*hybrid*' approach is based on a mix of experimental data and FEM-based simulation results. A reliable 3D-FEM model of a 4-poles 15 kW induction motor, with closed rotor slots, has been used to investigate the impact of a variable contact resistance on the inter-bar currents, rotor Joule losses, and the voltage drops along the bars, opening a new prospective for this complex phenomenon and its impact on the stray losses. Finally, the proposed methodologies are critically discussed and the obtained results compared with other relevant research works.

Index Terms— **Induction motors, die-cast aluminum rotor cages, inter-bar currents, contact resistance, FEM modeling, non-destructive measurement method**

NOMENCLATURE

Δl	Length of the rotor tooth layer
Δw	Thickness of the rotor core layer
ΔI_e	Current in the elementary rotor tooth layer Δl
ΔV_e	Voltage across the rotor tooth layer Δl
γ, γ_1	Electrical conductivities of the lamination
γ_{Al}	Electrical conductivity of the rotor bar
L_e	Rotor core length of the layer between adjacent bars
R_e	Rotor core layer resistance
R_c	Rotor bars/laminations contact resistance
$\Delta u(x)$	Instantaneous voltage in the elementary bar part
ΔR_b	Resistance of elementary bar part
$i(x)$	Instantaneous current in elementary bar part
Δx	Length of the elementary rotor bar part
$S(x)$	Cross-section of the elementary rotor bar part
u_{bar}	Total voltage drop along rotor bar

I. INTRODUCTION

ELECTRICAL machine designers are currently facing many types of challenges to meet the stringent requirements imposed by international standards. One of them is to increase the motors efficiency, leading to a reduction in electricity consumption by electric motors. Aluminum-cage induction motors are widely used in industry, transportations, and household appliances. Even if induction motors have been modeled in general for over a century, refinements to improve their performance are continuously ongoing [1]. From this viewpoint, the estimation and reduction of rotor Joule losses have been one of the topics studied for a long time. Correct estimation of these losses requires, among others, the knowledge of inter-bar current flow, which results from the correct estimation of the rotor bar-rotor lamination contact resistance [2].

To overcome the mentioned challenge, it is not only required to limit the well-known classic losses (like the Joule losses in the stator and rotor windings and the iron losses in the magnetic cores), but also to minimize any source of additional losses, including those caused by currents flowing among the bars of the rotor cage. Although for medium sized motors the total stray losses constitute a very small percentage of the input power, the share of Joule losses resulting from the inter-bar currents can reach even 30% of these losses [3], [4]. Therefore, it is justified to make further attempts to achieve maximum motor efficiency, solving this interesting problem from different perspectives than the past. For this reason, the authors recently decided to methodologically approach the phenomenon both from a theoretical and an experimental viewpoint [5], [6]. In particular, the novelty of the method consists in the possibility of correlating measurable signals (i.e. the voltage that appears on the surface of the rotor during "simple" locked rotor tests) with the contact resistance. According to the best knowledge of the authors, this non-destructive method to identify the bar-core contact resistance is new and is not yet discussed in the literature.

The present paper summarizes the previous activities, and it is organized as follows. Starting from a review of the published methods for determining the rotor bar-lamination contact resistance, the description of the FEM model used for inter-bar currents estimation is reported. Then, the proposed '*hybrid*' method for the contact resistance estimation is point-to-point presented, together with selected results of measurements and FEM simulations. Finally, the main outcomes of the research are outlined and critically discussed.
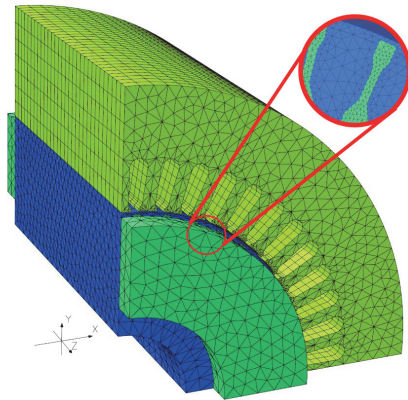
Fig. 1. The 3D-FEM model with mesh (stator winding is invisible); details of the dense mesh used in the locked rotor simulations.
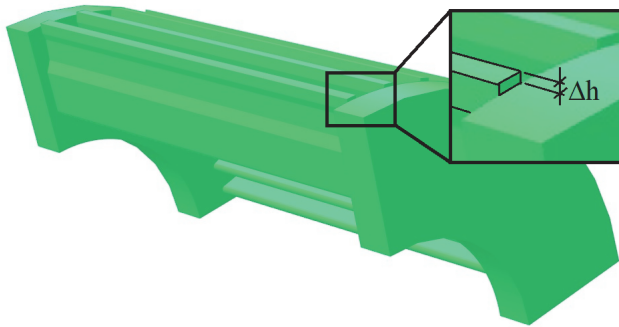

Fig. 2. The unskewed rotor cage 3D-FEM model.

II. LITERATURE REVIEW

The correct quantification of the effects of inter-bar currents lies in the availability of a reliable value of the rotor bar-lamination contact resistance. Unfortunately, the direct measurement of this contact resistance is incontestably not trivial. In particular, its value is very small (i.e. in the range of few tens of micro-Ohm), making the development of measurement methodologies hard. Additionally, the manufacturing technologies of squirrel-cage rotors have a significant impact on the contact resistance values. Therefore, different values of contact resistance can be measured depending on the selected bar for testing, because it is difficult to clearly determine the current path during tests [7]. The methods already presented in the literature for measuring the contact resistance can be roughly subdivided in non-destructive ([8]-[11]), and destructive methods in which specific rotor parts are removed to directly apply a *dc* supply to the cage bars [12], [13].

Usually, non-destructive methods inject a *dc* current between the shaft and the cage rings. Therefore, the determination of the contact resistance is often based on the adoption of a specific current path and the measurement of the voltage drop along this path. However, according to [8] the results obtained by using different non-destructive methods can vary up to 10 times, leading to very inaccurate computation of the inter-bar currents and related losses. The main reason for large variations can be found in the casting technologies used for the aluminum rotor cages. It is worth mentioning that for the contact resistance estimation, other non-invasive methods based on different approaches have been proposed; for instance, the use of

calorimeter tests and the motor equivalent circuit ([14]), or dedicated iron loss measurements [7].

It should be pointed out that the indirect, non-destructive method described in [15] proposes to use torque measurements during the motor start-up to estimate the average value of the contact resistance, as the presence of inter-bar currents affects the shape of torque versus speed dynamic curve. This study confirms the authors' finding that locked rotor operations (exploited in the proposed '*hybrid*' method) can be usefully considered for developing new identification techniques of the contact resistance. However, in all the presented approaches, the actual paths of the injected currents are unknown, and the definition of equivalent electrical circuits does not only sound arbitrary, but also does not give a full answer to the problem.

In the proposed non-destructive approach, a new hybrid method is presented to estimate the bar-rotor lamination contact resistance: the approach is relatively simple, and it is based on the measurements of the voltage induced on the rotor surface in locked rotor condition. In detail, the contact resistance is estimated by comparing measurements with results extracted by accurate 3D-FEM models. Since these type of numerical models are today commonly used to evaluate the inter-bar current distributions and the related losses, the proposed approach does not require extra computational resources for the identification of the contact resistance.

III. THE 3D-FEM MODEL

Even if the value of the contact resistance between bars and lamination is available, further problems must be solved from the practical point of view: e.g. how to compute the inter-bar currents and the related additional losses. The basic per-phase equivalent circuit can be used ([2]), but the today's approaches for the inter-bar computation are based on numerical FEM simulations, such as 2D multi-slice models ([2], [16]-[22]) or 3D-FEM models ([23]-[25]).

Recently, the authors implemented the 3D-FEM model of a 400V-50Hz, 4-poles, 15 kW induction motor, having closed rotor slots, for investigating its efficiency [1]. Both skewed- and unskewed-bars rotors are available for simulations and testing. The very good agreements observed between measurements and simulations demonstrated the accuracy and reliability of the developed 3D-FEM model for the description of the motor operations. Consequently, the model shown in Fig. 1 and Fig. 2 has been now adapted to account for the presence of the inter-bar currents, although the authors are aware that the calculation time is considerably extended compared to the other aforementioned approaches.

An important problem solved by the authors was how to model the laminated rotor core without the simplifications assumed in previous researches. Although today it is technically possible to model each magnetic sheet and its insulation, the need to simulate uneven current and flux density distributions would require hyper-power calculation systems. These computation facilities are not currently available to the authors. Fortunately, the used FEM software allows to define an anisotropic electric conductivity; as a consequence, assuming the electrical conductivity of the rotor core equal to zero for the Z-axis (see Fig. 1), the currents cannot flow in this direction, which is reasonably equivalent to have a laminated rotor core.

The skin effect that occurs both in the aluminum bars and in the rotor lamination parts where the inter-bar currents flow, plays an important role for the correct physical description of the investigated phenomena. Therefore, very dense mesh constituted by second order elements have been used in these two regions. To limit the computation time, only a fourth of the motor has been modeled, resulting in 1.3 million of elements. An important feature of the used commercial software is the possibility of solving the electromagnetic problem (i.e. the field distributions and the electromagnetic torque) taking in to account the currents induced in the model regions, even in the rotating elements. Accordingly, the used solver enables simultaneous solving of equations representing the electromagnetic field, electrical circuits and mechanical dynamics, if needed. Complete details about the problem definition with the inter-bar currents can be found in [5].

A. Model and Simulation Setup

For the simulations, the stator windings were supplied with a sinusoidal voltage with increasing amplitude, according to a 40 ms ramp. The adoption of a ramp voltage significantly reduces the time to reach the steady-state solution. For example, using the proposed technique, the locked rotor simulations require '*only*' 150-190 hours, depending on the rotor topology (i.e. the skewed or unskewed cages).

The eddy currents in the stator core are nullified assuming an electrical conductivity equal to zero, while anisotropic electrical conductivities (variable in the X- and Y-axis, and null in the Z-axis direction) have been considered for the rotor core material. As it will be articulated in Section IV, a variable rotor conductivity is used to emulate a variable value of the bars-laminations contact resistance. For the cage material, the electrical conductivity has been defined equal to 30 MS/m; finally, a non-linear magnetization curve was used both for the stator and the rotor core material. The calculations were executed for locked rotor condition as well as for load operations at 1490 rpm. In particular, for the simulations of the locked rotor tests, a reduced voltage has been defined (e.g. to reach the rated stator current for the non-conducting rotor core case); the same voltage value has been used to analyze all the other conducting rotor core cases.

(a)

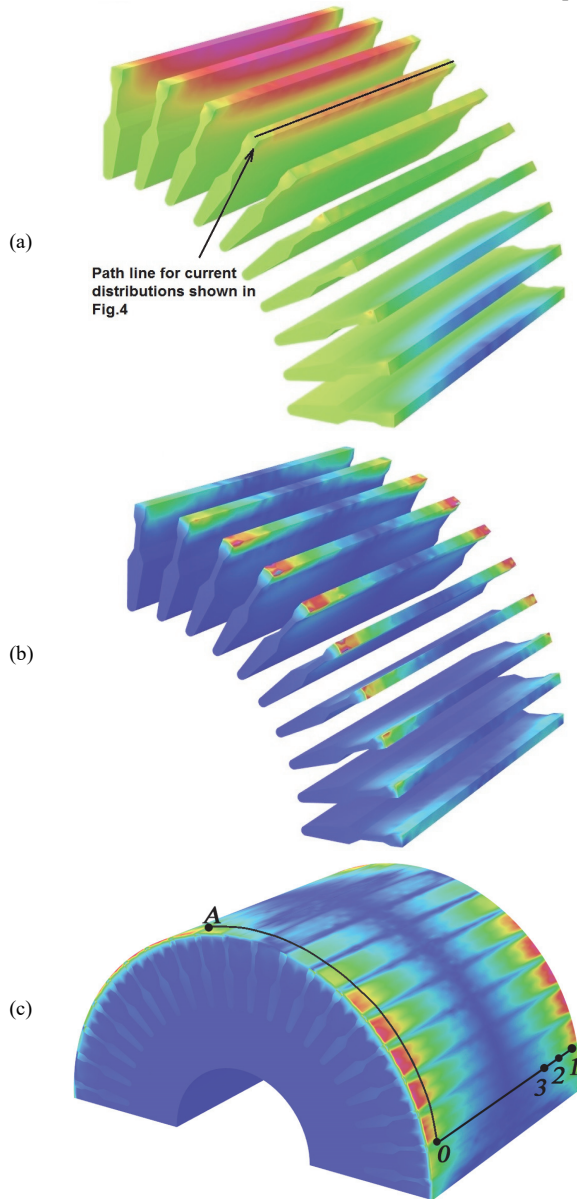Path line for current distributions shown in Fig.4

(b)

(c)

Fig. 3. Current density distributions in the rotor bars and in the rotor core in locked rotor condition (50 Hz, bar current = 80 A, unskewed bars): (a) axial direction component, (b) & (c) in circumferential direction (perpendicular to the bars).
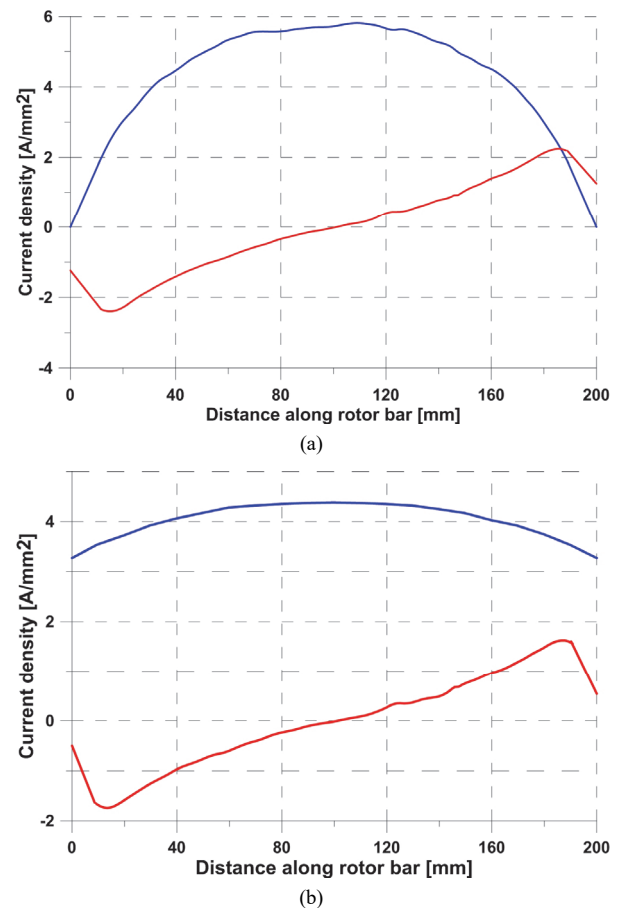

(a)

(b)

Fig. 4. Current density distributions at the upper surface of the bar carrying the maximum current (same conditions as Fig.3, contact resistance = 24μΩ): (a) on the path shown in Fig.3.a, (b) on a line parallel to the previous path positioned inside the bar at the distance Δh shown in Fig. 2 – Blue: component along bar, red: component perpendicular to the bar.
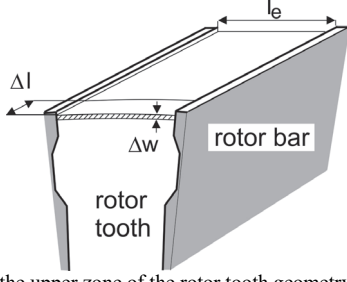
Fig. 5. Sketch of the upper zone of the rotor tooth geometry.

Obviously, the rated voltage has been used to study the load operations. Just as an example, Fig. 3 shows the current density distributions computed in the bars and in the rotor core in locked rotor condition for the 15 kW induction motor used in the tests.

IV. THE PROPOSED HYBRID METHOD

The inter-bar currents and the related additional Joule losses (including those due to the uneven current distribution along the bar axial direction, especially in locked rotor conditions) can only be computed by means of FEM models. Thus, it is straightforward to base a non-invasive method to estimate the bars-rotor contact resistance on 3D-FEM analyses, replicating as much as possible measured data. However, the definition of a non-invasive procedure based on a mixed use of experiments and FEM models leads to two '*philosophical*' problems: (i) the FEM model must be able to take into account the contact resistance, and (ii) measurable signals representative of the contact resistance value must exist.

Because of the used commercial FEM package does not allow a direct definition of contact electrical resistance among different regions, a different modeling approach has been used to solve the first problem. However, even if the FEM packages allow for a direct definition of the contact resistance, the selection of its value is not straightforward because it depends by the specific technology used for the rotor production and the related factors (i.e. rotor casting technology, surface roughness, average thickness, and so on). In particular, in the proposed approach, to emulate a variable value of the contact resistance from zero to infinite, the electrical conductivity of the rotor core material in the X- and Y-direction has been changed in a range from 2 MS/m to 0 MS/m (where 2 MS/m is the value reported in the lamination datasheet). The resultant value of the contact resistance can be extracted by the simulation results using the steps (1)-(3) reported in Section IV.A.

To solve the second problem, it is necessary to observe Fig. 4a carefully. In fact, this figure puts in evidence that the inter-bar current phenomenon leads to uneven current distributions on the upper bar surface (i.e. along the path line shown in Fig.3a). As a consequence, particular trends of the voltage induced on the rotor surface are expected, both in axial and circumferential direction.

In particular, as shown in Fig. 4a, the current density component along the rotor bar tends to be zero at both the bar ends or – equivalently – the ends of the core. This is due to the fact that the upper surface of the bar, on which the path line shown in Fig. 3a was positioned, is slightly above the upper surface of the rotor ring – see Fig.2.
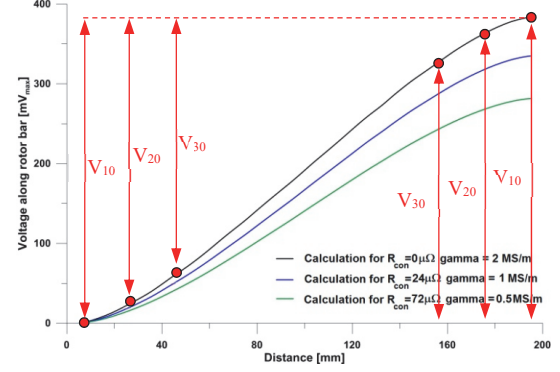

Fig. 6. Example of the voltage signals along the bar computed by (7) for different contact resistance during the locked rotor test simulations (with rated stator current).

As shown in Fig.4b, if the path is parallel translated inside the bar of the distance Δh, which if specified in the zoom of Fig. 2, the axial current components are no longer zero. This aspect is not particularly relevant for the component perpendicular to the bar. It is more important to notice that there is the rotor ring, which drains the perpendicular current component. As a result, the maximum current density of the perpendicular component is located at a distance of $10 - 12$ mm from the core ends; it was observed that this distance depends on the ratio of the ring and lamination resistances.

The particular trends of the voltages that appear on the rotor surface can be easily obtained both during the post-elaborations of the FEM simulations – see (4)-(7) – and by measurements on existing prototypes. In any case, the shape of these trends can be put in correlation with the contact resistance value, solving the second '*philosophic*' problem. Obviously, the voltages that appear on the rotor surface can only be measured if the rotor is not rotating, opening the way at the proposed non-invasive measurement method based on '*ad-hoc*' locked rotor test.

A. Post-elaboration of the FEM results

Under 50 Hz locked rotor conditions and due to the well-known skin effect, the currents in the bars, as well as the inter-bar currents in the laminations, are located in the core regions close to the air-gap. Therefore, the upper tooth region reported in Fig. 5 has been taken into consideration for the description of the contact resistance.

First of all, it has been assumed that the contact resistance is the same for each '$\Delta w \cdot \Delta l$' section, both on the left and on the right ends of the considered elementary layer. For the considered elementary tooth part, the current (ΔI_e) and the applied voltage (ΔV_e) can be extracted by the FEM simulations. Thus, the electrical resistance of the considered element (R_e) can be written in accordance to (1),

$$R_e = \frac{\Delta V_e}{\Delta I_e} = \frac{l_e}{\gamma \cdot \Delta w \Delta l} \qquad (1)$$

The case of negligible contact resistance between bars and laminations is assumed for the electrical conductivity of the lamination (e.g. 2 MS/m for the case of study). This value is generally available in the lamination catalogue. Therefore, the lamination conductivity γ_1 is decreased, in a discrete way, from 2 MS/m to zero in order to account for an increasing contact resistance R_c in the FEM models, in accordance to (2).

$$R_c = \frac{1}{2}\left(R_e(\gamma_1) - R_e(\gamma)\right) = \frac{1}{2}\frac{l_e}{\Delta w \Delta l}\left(\frac{1}{\gamma_1} - \frac{1}{\gamma}\right) \quad (2)$$

It is immediate to rewrite (2) as reported in (3).

$$R_c = \frac{1}{2}R_e\left(\frac{\gamma}{\gamma_1} - 1\right) \quad (3)$$

The first estimation method of the contact resistance uses the voltage waveform that appears along the cage bar during locked rotor conditions. Neglecting the voltage drop in the radial direction above the bars, the same voltage is directly measurable on the surface of the rotor. Therefore, it is necessary to determine the formulation of the voltage drop along the path shown in Fig. 3a as a function of the current density in the rotor bar (the component along the bar, shown in Fig. 4a). As the currents flowing in the elementary parts of the bar are in phase with each other in the time, it possible to arithmetically sum up voltage drops induced in each elementary part to get the total voltage on the current path. The calculation has to be carried out at the time instant when the maximum current flows in considered rotor bar, that will correspond to the maximum voltage value along the bar. Of course, this voltage is variable over time. For a fixed time instant, the voltage drop along the elementary fragment of the bar can be computed by (4), where $i(x)$ and $\Delta R_b(x)$ are the current and resistance of the elementary bar part. The x-coordinate is oriented along the axial direction.

$$\Delta u(x) = \Delta R_b(x) \cdot i(x) \quad (4)$$

$$\Delta R_b = \frac{\Delta x}{\gamma_{Al} \cdot S(x)} \quad (5)$$

The $S(x)$ cross-section can be determined by the FEM model whereas the current along rotor bar and the total current in the bar can be determined from simulations. Taking into account the current density definition $j(x) = i(x) / S(x)$, and observing that Δx can be substituted by the Δl shown in Fig.5, (4) can be rewritten as shown in (6), and the total voltage along the bar computed in accordance to (7). For the considered case study, examples of the signals induced in axial direction over a rotor bar are shown in Fig. 6. The figure also reports the contact resistance values estimated by (3).

$$\Delta u(x) = S(x) \cdot j(x) \frac{\Delta x}{\gamma_{Al} \cdot S(x)} = j(x)\frac{\Delta l}{\gamma_{Al}} \quad (6)$$

$$u_{bar} = \sum \Delta u(x) = \sum j(x)\frac{\Delta l}{\gamma_{Al}} \quad (7)$$

In addition to the voltage drop over a bar, also the voltage induced over a polar pitch (e.g. on the arc 'A0' shown in Fig. 3c) can be extracted by the FEM simulations. The amplitude of this signal represents the average spatial value of the voltage drops over a polar pitch length, which is proportional to the current flowing through the laminations.

By suitably adapting (7), the integral sum of the current density waveform inside the lamination can be computed at the selected time instant – see Fig. 7. For a correct signal extraction, the amplitude of the integrated current density waveform must be scaled of $2 / \pi$, computing the average values over its half-period of change. Finally, it should be noted that the distance of the arc '0A' from the rotor core end (see Fig. 3c and the distribution in Fig. 4a) is a very important parameter to fairly compare simulations and experiments. It should be noted that the voltages that appear on the rotor surface are not due to the magnetic flux in the airgap (and the related spatial harmonics), but they are the result of specific current components flowing close to the upper bar surface. Also, the '*spatial*' harmonics in the current density waveform shown in Fig. 7 are not due to the

rotating fields at the airgap, but to the stator winding arrangement (e.g. the considered motor is equipped with a short-pitch double-layer winding having low mmf harmonic content) and the selected time instant.
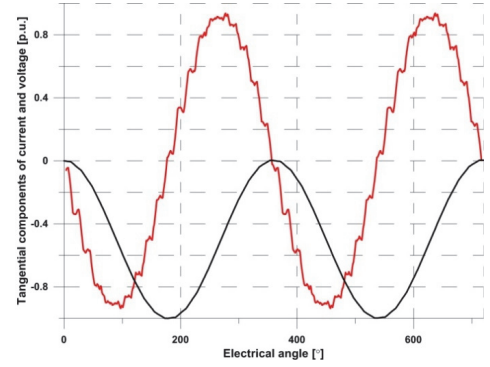

Fig. 7. Current density (red) and integrated current density (black, equal (7) except for the Δl and γ_{Al}) – locked rotor test simulation, 50 Hz supply.
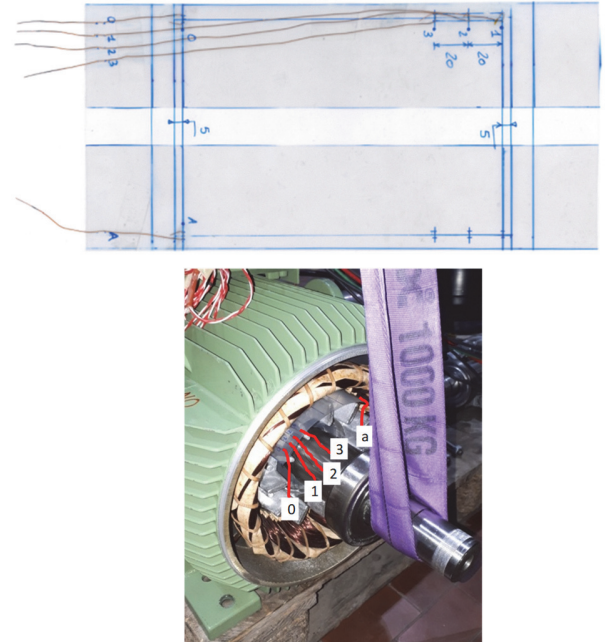

Fig. 8. The voltage probe used to measure the voltage induced on the rotor surface (on the top) and the probe inserted in the motor air-gap (on the bottom).

B. Induced voltage trend reconstruction using few points

Due to the domain symmetry and observing that the bending of the voltage trends mainly occurs close to the rotor core ends, it is possible to describe the trends of the rotor voltages induced over the bar using very few '*measurements*' points and the self-understandable graphical procedure depicted in red in Fig. 6. In particular, for the induction motor under investigation, only three voltage signals are enough to obtain a good estimation of the '*bending*' of the trends [5].

It should be also noted that for accurate estimations, the measurement points '0', '1' and 'A' must be positioned as close as possible to the ends of the rotor core. In particular, the authors positioned these three contact points at 5 mm from the core ends, while the distance '1'-'2' and '2'-'3' is equal to 20 mm (see Fig. 3a). This solution makes easier, or better to say feasible, the execution of the proposed locked rotor test.
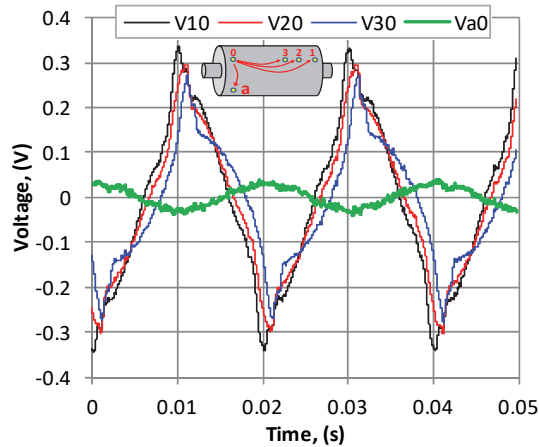
Fig. 9. The measured voltage drops on the unskewed rotor surface in locked rotor condition (three in axial and one in circumferential direction, 50 Hz, reduced supply voltage to get the rated stator current).
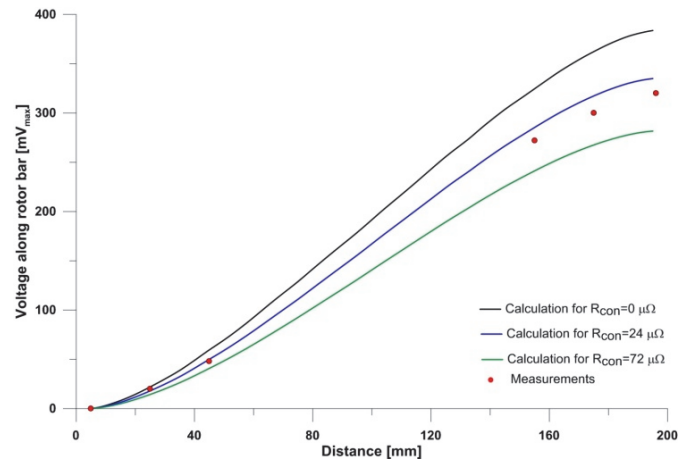

Fig. 10. The comparison of the simulated and measured induced voltage on the rotor surface in axial direction (locked rotor condition, 50 Hz supply).

In addition, during the proposed tests the machine works like a transformer preventing the high-frequency components in the voltage waveforms (e.g. due to the rotation and the slotting).

V. MEASUREMENTS AND CONTACT RESISTANCE ESTIMATION

Measuring the aforementioned voltage signals is not a simple task for several practical reasons: (i) they are very small, (ii) the air gap of induction machines is generally very thin, and (iii) it is very difficult to electrically connect copper wires to lamination sheets in the contact points 'A, 0, 1, 2, 3' defined in Fig. 3a. For example, the air gap of the prototype (a 4-poles 15 kW induction motor) is only 0.4 mm, and insertion and placing of conventional voltage sensors in the air gap were not possible. For this purpose, the special voltage '*probe*' shown in the top of Fig. 8 has been built and inserted in the air gap of the motor removing the two end-caps. The probe is made by a flexible plastic sheet, with two edges folded on themselves to contain very thin copper wires. The wires come out of the sheet plastic through small holes drilled in the five contact points. The thickness of the probe resulted approximately equal to 0.4 mm, and the removal of the two end caps was mandatory to insert easily the probe in the air gap. However, to guarantee good electrical contacts and the rated value of the air gap thickness, the rotor has been raised by sticking the probe with the stator (see Fig 8, on the bottom). The tips shown in this figure allow using a digital oscilloscope to acquire the signals. Finally, the measured voltage drops among the selected contact points are reported in Fig. 9. These signals have initially been measured using the unskewed rotor and imposing the rated current in the stator winding at 50 Hz. Then, their fundamental components have been computed. In accordance with the graphical procedure depicted in Fig. 6, the amplitude of these three fundamental voltages (in the time) allows positioning (in the space) the red points included in Fig. 10.

Comparing in a linear way the '*bending*' of the measured curve with the computed ones (for 24 μΩ and 72 μΩ), the contact resistance determined on the basis of the performed measurements is estimated equal to 36 μΩ. The amplitude of the fundamental component of the voltage V_{A0} shown in Fig. 9 is equal to 38 mV, as it could be computed by FEM simulations enforcing a contact resistance of 40 μΩ.

Taking into account the technical difficulties and signal distortions occurring during the measurement, both the axial and circumferential voltage signals allow comparable estimations of the contact resistance existing between the bars and laminations. It is important to remark that the obtained values for the contact resistance are within the ranges given in previously published studies [2], [14], [27].

The proposed locked rotor test has also been repeated using the skewed rotor (the skew is equal to one rotor slot pitch), obtaining similar results even if only stator current values up to 0.6-0.7 p.u. were explored. In fact, during the test it was not possible to reach the rated current because the rotor started to vibrate, making impossible to acquire the signals with the test setup shown in Fig. 8.

As the same technological process used to produce the two rotors is the same and the squirrel cages have been die-casted in rapid sequence (i.e. the aluminum electrical properties are reasonably the same), the estimated values prove that the bars-core contact resistance does not depends by the skewing. However, the following FEM analyses show that the rotor skewing impacts both on the inter-bar current distributions and on the extra losses.

VI. INTER-BAR CURRENTS AND RELATED LOSSES

As stated in the introduction, using the contact resistance estimated by the proposed '*hybrid*' method, the distributions of currents in the rotor bars and in the rotor core can be determined. In particular, both locked rotor conditions and 1490 rpm operations at nominal torque have been investigated. To better understand the inter-bar current distributions in the rotor core during different working conditions, the two reference planes shown in Fig. 11 have been considered: one in the bar and the other in the center of the tooth.

In locked rotor condition, the current component perpendicular to the second reference plane is shown in Fig. 12, while Fig. 13 shows the current distribution in the lamination plane. These figures confirm that at high slip frequency (i.e. 50 Hz) the inter-bar currents are located in the periphery of the rotor core.
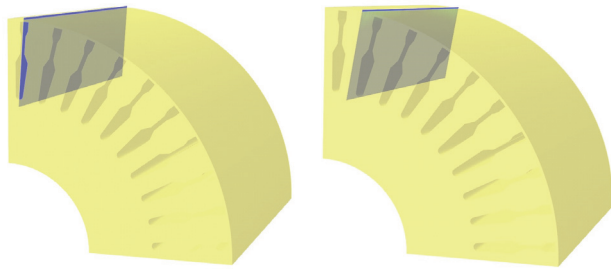
Fig. 11. Reference planes for the inspection of the bar current distribution (on the left) and the core current distributions (on the right).

Fig. 12. Current density distribution for the unskewed rotor cage (component in the lamination plane – Fig. 11 on the right – in locked rotor condition).
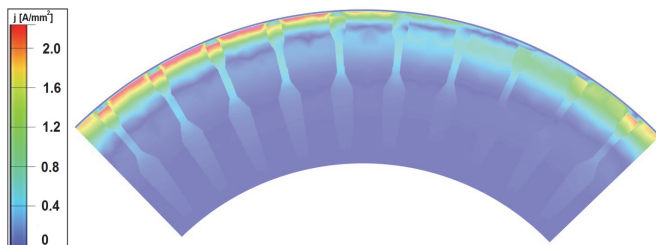

Fig. 13. The current density distribution for unskewed rotor cage over a pole pitch: component in the lamination plane in a slice cut at distance of 5 mm from rotor ring (50 Hz locked rotor condition).

Fig. 14. The current density distribution for unskewed rotor cage: component in the lamination plane, over a pole pitch in a slice plane at the distance of 40 mm from the ring (at specified time moment, load condition, 1490 rpm).

Fig. 15. The current density distribution for skewed rotor cage: component in the lamination plane, over a pole pitch in a slice plane at the distance of 40 mm from the ring (at specified time moment, load condition, 1490 rpm).

a)

b)

Fig. 16. Current density distribution in the rotor bar in locked rotor condition: (a) perpendicular and (b) parallel component to the reference plane shown on the left of Fig.11.

a)

b)
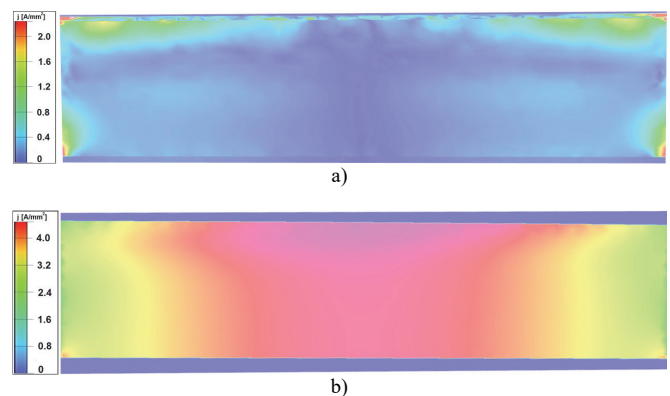
Fig. 17. Current density distribution in the rotor bar under rated load operation at 1490 rpm: (a) perpendicular and (b) parallel component to the reference plane shown on the left of Fig.11.

The phenomenon of the inter-bar currents depends also by the frequency of the induced currents, and – as a consequence – their distributions change with the load torque and rotational speed. As an example, the current density distributions of the component 'in the lamination plane' are shown in Fig. 14 and Fig. 15 for the unskewed and skewed rotor at the rotational speed of 1490 rpm. In both cases, the electrical conductivity is equal to 0.8 MS/m, which corresponds to the estimated contact resistance of 36 μΩ. At this speed, the fundamental frequency of the induced phenomena in the rotor is approximately 0.3 Hz. It is evident that at 1490 rpm the distributions are very different with respect to the ones in locked rotor condition previously presented. In fact, at low slip frequency the '*penetration*' of the inter-bar currents is bigger, and they flow in the whole rotor slot domain. In addition, the impact of the skew on the area in which inter-bar currents flow is even more visible (see Fig. 15). However, inter-bar currents flowing in core regions located close to the air gap are still present, as they are induced by the spatial harmonics of the induction in the air gap. For comparison, Fig. 16 and Fig. 17 show current density distribution in rotor bar, in locked rotor condition and 1490 rpm.

From an engineering point of view, it is interesting to estimate the amount of additional Joule losses resulting from the inter-bar currents, especially in caged induction motors.
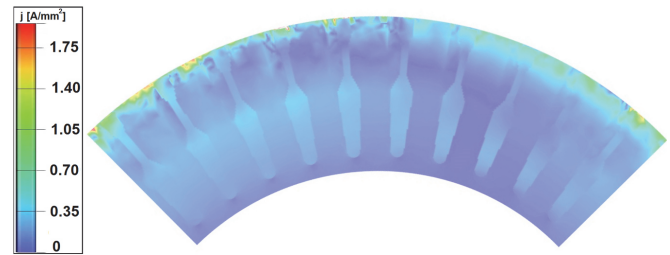
TABLE I
ROTOR CORE JOULE LOSSES INCLUDING THE INTER-BAR PHENOMENON AT
LOAD CONDITION (RATED VOLTAGE, 1490 RPM)

Contact resistance, ($\mu\Omega$)	Skewed rotor, (W)	Unskewed rotor, (W)	Skewed/ Unskewed
0	271	41	6.6
4	215	35	6.2
9	165	29	5.8
14	121	23	5.2
24	83	19	4.4
36	65	17	3.9
44	53	15	3.5
72	30	12	2.4
105	16	11	1.5
200 ($\approx\infty$)	10	10	1.0

Even if with the proposed hybrid method, a reliable value of the contact resistance can be evaluated for existing prototypes, the computation of the Joule losses requires further simulations as the distributions of the magnetic field in the rotor core and the currents in the rotor bars depend on the operating conditions of the machine. In fact, under load conditions, the distributions are completely different from those observed during the locked rotor test simulations – see Fig. 16 and Fig. 17.

As selected contact resistance values can be properly enforced the FEM model changing the conductivity of the rotor laminations, it is possible to compute the rotor core losses when the machine is running. Once again, it should be emphasized that the rated voltage and a speed of 1490 rpm have been assumed. The uneven distribution of currents flowing through the core must be taken into account for the computation of the Joule losses in the rotor core. In fact, the used software package determines the Joule losses in each core element based on the knowledge of the current density and the electric field strength in its volume. Then, the elementary losses are added and the total core losses are obtained. It should be noted that the total losses include several components that cannot be separated by the used model, such as the losses originating from inter-bar currents and the rotor surface losses generated by higher spatial harmonics of the flux density in the air gap. Furthermore, based on the aforementioned definition of contact resistance, it is immediate to observe that the core Joule losses computed using an electrical conductivity of the core material lower than 2 MS/m correspond to the Joule losses that can be computed using the real electrical conductivity (of 2 MS/m) plus the Joule losses dissipated in the contact resistance. The computed Joule losses in the rotor core are reported in Table I, both for the skewed and unskewed rotor. As expected, the core Joule losses increase when the contact resistance decrease. For infinite contact resistance the inter-bar currents are negligible, and only the eddy current losses on the rotor surface are active. Using a very dense mesh on the rotor periphery, these losses are estimated to be equal to 10 W (for the specific geometrical dimensions of the tested motor), independently by the rotor structure. In presence of inter-bar currents, higher rotor core Joule losses have been observed for the skewed rotor (up to 6-7 times the losses of the unskewed rotor cage, for the limit case of negligible contact resistance) [28], [29]. However, in unskewed cages the Joule losses in the bars due to the current ripples induced by the spatial flux density harmonics are bigger than the ones in the skewed cage counterpart [1], [26].

VII. DISCUSSION

The present study deals with the problem of inter-bar current distribution, which results from the presence of rotor bar/laminations contact resistance, as well as the frequency of the magnetic field that generates them. These currents introduce additional power losses, both in the rotor cage bars as well as in the rotor core. The relation of these losses to all other components of motor power losses is generally known, but – considering that nowadays designing energy-saving electric motors is enforced by imposed rules – a deep knowledge of these phenomena is the reason for undertaking research in this area. For this purpose, the proposed method for estimating the contact resistance was compared to other methods described in the literature. It should be emphasized that the proposed hybrid method is a new non-invasive method, which is currently particularly desirable by engineers. This method combines a relatively simple measurement of voltage signals and FEM model. The model, by changing the electrical properties of laminations, determines the waveforms and amplitudes of current density at specific places on the rotor surface, expecting to achieve values comparable to those measured.

The limited disadvantages of the proposed methodology are: (i) the users must have good skills in 3D-FEM modeling, (ii) quite long calculation times are requested, and (iii) the problem for the positioning of the voltage sensor to measure the induced voltage signals in the rotor surface must be solved case-by-case.

From a practical point of view, two conclusions should be drawn from the implementation of measurements. First at all, being the rotor slots closed, during the locked rotor test it is not possible to measure the voltage drop on the upper surface of the bar, but only on the rotor surface. However, on the basis of the inter-bar currents distributions presented in the paper, it is possible to assume negligible voltage drops between the bar top and rotor surface (i.e. in the radial direction). Then, the voltage drop trends along the paths inside the bar or on the rotor surface should be practically the same. Secondly, the small air gap of the induction motor prototype is 0.4 mm only, making it impossible to be directly 'touch' with the standard oscilloscope probes the four measuring points on the rotor surface. It is important to remark that it is not possible to weld thin copper wires in the selected rotor positions. For this reason, the authors produced a special voltage probe that guarantees a good electrical contact in the measuring points. It should be emphasized that such an approach of the contact resistance estimation is completely new, and it has not yet been described in the literature.

A straightforward validation of the 'goodness' of the proposed method is the comparison with the results previously published by other researchers. Being aware that the contact resistance depends on many technological parameters (many of them having a statistical nature), it should be checked if the determined contact resistance is within the range of results provided by other researchers. However, there is no consistency in the presentation of results: some researchers show the resistance value, while others present the resistivity. Nevertheless, in literature it is possible to find results that well agree with the obtained values [14].

As reported in several studies, the contact resistance depends on the temperature [2]. From this view point, as the locked rotor

test has been quickly performed, for the simulations the material parameters of the bars were set as for the nominal temperature, while the lamination parameters as for the ambient temperature (considering the high heat capacity of the laminated core). This assumption allowed having a good replication of the experiments with the FEM models. However, being the methodology validated, the definition of a reasonable correlation between the contact resistance and the working temperature will be the subject of future researches.

Finally, thanks to the proposed approaches (including the methodology for the contact resistance estimation), the authors can compare the obtained rotor core loss with those calculated by other researchers, for motors having similar dimensions and rated power. In particular, for the considered case study, the estimated Joule losses in the rotor core well agrees with the results presented in [10], [23], [25]. With respect to the current distributions in the rotor core and cage bars, the study demonstrates that they are very different moving from locked to rotating rotor condition. Therefore, in order to avoid estimation errors, the authors suggest to avoid to extrapolate the losses in rated operations (i.e. for a fixed speed and load torque), starting from the analyses carried out in locked rotor conditions.

VIII. CONCLUSION

The work provides an interesting insight into the inter-bar current phenomena that occurs in die-cast cages of induction motors, for which direct measurements are generally not possible. In particular, a parametric analysis (changing the electrical conductivity of the rotor core laminations) of the voltage drops on the rotor surface demonstrates the possibility of estimating realistic values of the contact resistance between bars and laminations. Based on these investigations, a tailored locked rotor test procedure has been proposed, pursuing the definition of a new non-destructive mixed numeri-cal/experimental approach for accurate determinations of the contact resistance. Finally, the authors developed original approaches for the implementation of precise 3D-FEM models which are able to describe the inter-bar currents in skewed and unskewed rotor cages and their impact on the additional rotor Joule losses.

REFERENCES

[1] A. Cavagnino, S. Vaschetto, L. Ferraris, Z. Gmyrek, E. B. Agamloh, and G. Bramerdorfer, "Striving for the Highest Efficiency Class with Minimal Impact for Induction Motor Manufacturers," in *IEEE Trans. on Ind. Applic.*, vol. 56, no. 1, pp. 194-204, Jan.-Feb. 2020.

[2] D. G. Dorrell, TJE Miller and C. B. Rasmussan, "Inter-bar currents in induction machines", *IEEE Trans. on Ind. Applic.*, Vol 39, No 3, 2003, pp 677 – 684.

[3] A. R. Hagen, A. Binder, M. Aoulkadi, T. Knopik, and K. Bradley, "Comparison of measured and analitycally calculated stray losses in standard cage induction machines", Proc. Int.. Conference on Electrical Machines, pp.1-6, 2008.

[4] H. Nishizawa, K. Itomi, S. Hibino, and F. Ishibashi, "Study on reliable reduction of stray load losses in three-phase induction motor for mass production," *IEEE Trans. Energy Conversion*, vol. EC-2, pp. 489-495, 1987.

[5] Z. Gmyrek, A. Cavagnino and S. Vaschetto, "FEM Analysis of the Inter-Bar Currents in Induction Motors Aimed at Estimating Contact Resistance," 2019 IEEE International Electric Machines & Drives Conference (IEMDC), San Diego, CA, USA, 2019, pp. 1532-1538.

[6] A. Cavagnino, S. Vaschetto and Z. Gmyrek, "Hybrid Method for Measuring Rotor Bar-Lamination Contact Resistances," 2019 IEEE Energy Conversion Congress and Exposition (ECCE), Baltimore, MD, USA, 2019, pp. 2335-2340.

[7] A. Nakahara, S. Kikuchi, K. Nishihama, T. Miyoshi and K. Daihatsu, "Interbar current losses in cage induction motors due to harmonic flux", Proc. Int. Electric Machines & Drives Conference, 2013.

[8] K. Dabala, "A new experimental-computational method to determine rotor-bar-iron resistance", Proc. Int. Conference on Electrical Machines, pp.69-72, 1996.

[9] S. Williamson and C.Y. Poh, "Inter-bar currents in cage induction motors", *IEE Proceedings - Electric Power Applications*, vol. 152, No 5, pp.1106-1112, 2005.

[10] N. Watanabe, T. Muramatsu, I. Hirotsuka, M. Nakamura, Y. Tsurumi at al, "Experimental study of inter-bar current effects in three-phase squirrel-cage induction motor", Proc. Int. Conference on Electrical Machines and Systems, pp.570-575, 2018.

[11] A. Stening, On inter-bar currents in induction motors with cast aluminium and cast copper rotors, Licenciate Thesis, 2010 (available at https://www.diva-portal.org/smash/get/diva2:325097/FUL-LTEXT01.pdf).

[12] D. Gersh, A. C. Smith, and A. Samuelso, "Measurement of inter-bar resistance in cage rotors", Proc. IEE Electric Machines Drives Conference, pp.253-257, 1997.

[13] G. Toke, P. L. Timar, P. Goszti, K. Toth, and G. Vincz, "Experimental determination of transverse resistivity of cast aluminium squirrel-cage," Proc. ICEM Conference, 1982, pp. 796-799.

[14] Y. N. Feng, J. Apsley, S. Williamson, A. C. Smith, and D. M. Ionel, "Reduced losses in die-cast machines with insulated rotors", *IEEE Trans. Ind. Appl.*, Vol. 46, No. 3, pp.928-936, 2010.

[15] A. Stening, C. Sadarangani, "Starting performance of induction motors with cast aluminium and copper rotors including the effects of saturation and inter-bar currents", Proc. Int. Conference on Electrical Machines and Systems, 2009.

[16] D. G. Dorrell, P. J. Holik, and C.B. Rasmussen, "Analysis and effects of inter-bar current and skew on a long skewed-rotor induction motor for pump applications", *IEEE Trans. Magn.*, vol. 43, no. 6, pp.2534-2536, 2007.

[17] D. G. Dorrell, P. J. Holik, P. Lombard, H.-J. Thougaard, and F. Jensen, "A multisliced finite-element model for induction machines incorporating interbar current", *IEEE Trans. Ind. Appl.*, vol.45, no.1, pp.131-141, 2009.

[18] S. Williamson and A. C. Smith, "Equivalent circuits for cage induction motors with inter-bar currents," *Proc. Inst. Elect. Eng.-Electr. Power Appl.*, vol.149, no.3, pp. 173–183, 2002.

[19] R. Carlson, C. da Silva, N. Sadowski, Y. Lefevre, and M. Lajoie-Mazenc, "Analysis of the effect of inter-bar currents on the performance of polyphase cage-induction motors," *IEEE Trans. Ind. Appl.*, vol.39, no.6, pp. 1674–1680, 2003.

[20] C. Kral, A. Haumer, B. Kubicek, and O. Winter, "Model of a squirrel cage induction machine with interbar conductances", Proc. 7th Modelica Conference, pp. 861-867, 2009.

[21] A.Taheri, and S. Farshad, "Modeling and simulation of inter-bar currents using several 2d mecs in squirrel cage induction motors, Proc. Power Electronics, Drive Systems & Technologies Conference, pp.101-106, 2013.

[22] Y. Zhan, K. Kong, G. Xu, J. Kang, and H. Zhao, "Analysis of damper transient currents in salient-pole synchronous generator with skewed armature slots considering inter-bar currents", *IEEE Trans. Ind. Appl.*, vol. 55, no. 1, pp. 336-343, 2019.

[23] K. Yamazaki, and Y. Watanabe, "Interbar current analysis of induction motors using 3-d finite-element method considering lamination of rotor core", *IEEE Trans. Magn.*, vol.42, no.4, pp.1287-1290, 2006.

[24] J. Güdelhöfer, R. Gottkehaskamp and A. Möckel, "3D FEM approach to study the physics of inter-bar currents in induction machines", Proc. International Conference on Electrical Machines, pp.18-24, 2016.

[25] Y. Kawase, T. Yamaguchi, Y. Iwai, M. Akiyama, N. Toida, T. Furukawa at al, "Numerical analysis of skewed squirrel-cage induction motor taking into account interbar current using 3-D finite element method", The COMPEL Journal, vol. 36, No 1, pp. 378-384, 2017.

[26] K. N. Gyftakis, P. A. Panagiotou, and J. C. Kappatou, "Application of wedges for the reduction of the space and time-dependent harmonic content in squirrel-cage induction motors", *Journal of Computational Engineering*, vol. 2013, Article ID 657425, 2016.

[27] J. Gyselinck, J. Sprooten, L. Vandevelde and Xose Lopez-Fernandez, "Multi-Slice FE Modelling of Induction Motors Considering Broken Bars and Inter-Bar Currents", ISEF2005 Studies in Applied Electromagnetics and Mechatronics, Vol. 27, S. Wiak, A. Krawzcyk, Xose M. Lopez Fernandez (Editors), IOS Press (Publisher), pp.169-174, 2006.

This article has been accepted for publication in a future issue of this journal, but has not been fully edited. Content may change prior to final publication. Citation information: DOI 10.1109/TIA.2020.3028347, IEEE Transactions on Industry Applications

10

[28] A. M. Odok, "Stray-load losses and stray torques in induction machines," *Trans. Amer. Inst. Elect. Eng. III, Power App. Syst.*, vol. 77, no. 3, pp. 43–53, Apr. 1958.

[29] L. Serrano-Iribarnegaray and J. Martinez-Roman, "Critical review of the analytical approaches accounting for interbar currents and experimental study of ageing in two-speed asynchronous motors for elevator drives," *IEE Proc. Elect. Power Appl.*, vol. 152, no. 1, pp. 72–80, Jan. 2005.

Zbigniew Gmyrek received the PhD. and DSc. degrees in electrical engineering from Lodz University of Technology, Poland, in 1996, and 2006 respectively. His research interests included magnetic material modeling and measuring, and studying the impact of mechanical cut on the magnetic material properties. He is currently an ASSOCIATE PROFESSOR, at Institute of Mechatronics and Information Systems, LUT, Poland. He is the author of 120 scientific papers. Prof. Gmyrek is a reviewer of many scientific journals, including the IEEE Transactions on Industry Application, the IEEE Transactions on Industrial Electronics, the IEEE Transactions on Magnetics, IET Electric Power Applications, and SENSORS.

Silvio Vaschetto (S'10–M'13–SM'19) received his M.Sc. and Ph.D. degrees in electrical engineering from the Politecnico di Torino, Italy, in 2007 and 2011 respectively. He is currently an Assistant Professor at the Department of Energy, Politecnico di Torino. Dr. Vaschetto is involved in analyses and design of electrical machines for high performance drives for aerospace and automotive applications. Dr. Vaschetto is a member of the IEEE Industry Application Society (IAS) and the Industrial Electronics Society (IES). He is an Associate Editor of the IEEE TRANSACTIONS ON INDUSTRY APPLICATIONS and IET Electric Power Applications and regularly serves the scientific community as a Reviewer for several transactions, journals and international conferences.

Mostafa Ahmadi Darmani (S'19) was born in Tehran, Iran, in 1987. He received his M.Sc. degree in electrical engineering in 2013 from Azad University in Tehran, Iran. From 2013 to 2018, Mr. Ahmadi Darmani worked in Iran as an electrical engineer and consultant in different industries, and as an instructor in training centers. He is currently working towards his Ph.D. degree in electrical engineering with the Department of Energy at the Politecnico di Torino, Italy. His main research interests include design and analysis of electrical machines. He is a Member of the IEEE Industry Application Society and the Industrial Electronics Society. He is a reviewer for several IEEE Transactions and international conferences.

Andrea Cavagnino (M'04–SM'10–F'20) was born in Asti, Italy, in 1970. He received his M.Sc. and Ph.D. degrees in electrical engineering from the Politecnico di Torino, Italy, in 1995 and 2000, respectively. He is a professor at the Politecnico di Torino. He has authored or coauthored more than 200 papers, receiving four Best Paper Awards. His research interests include electromagnetic design, thermal design, and energetic behavior of electrical machines. He usually cooperates with factories for a direct technological transfer and he has been involved in several public and private research projects. Prof. Cavagnino is an Associate Editor of the IEEE TRANSACTIONS ON ENERGY CONVERSION, a Past Chair of the Electrical Machines Technical Committee of the IEEE Industrial Electronics Society, and a past Associate Editor of the IEEE TRANSACTIONS ON INDUSTRIAL ELECTRONICS, and the IEEE TRANSACTIONS ON INDUSTRY APPLICATIONS. He was Guest Editor of six Special Sections for the IEEE TRANSACTIONS ON INDUSTRIAL ELECTRONICS. Prof. Cavagnino was the technical program chair of the IEEE-IEMDC 2015 conference. He is a reviewer for several IEEE TRANSACTIONS and other international journals and conferences.